

The Berlin Exoplanet Search Telescope II. Catalog of Variable Stars. I. Characterization of Three Southern Target Fields.

T. Fruth¹, J. Cabrera¹, R. Chini^{3,4}, Sz. Csizmadia¹, C. Dreyer^{1,6}, P. Eigmüller¹,
A. Erikson¹, P. Kabath^{1,2}, S. Kirste¹, R. Lemke³, M. Murphy⁵, T. Pasternacki¹,
H. Rauer^{1,6}, and R. Titz-Weider¹

thomas.fruth@dlr.de

ABSTRACT

A photometric survey of three Southern target fields with BEST II yielded the detection of 2,406 previously unknown variable stars and an additional 617 stars with suspected variability. This study presents a catalog including their coordinates, magnitudes, light curves, ephemerides, amplitudes, and type of variability. In addition, the variability of 17 known objects is confirmed, thus validating the results. The catalog contains a number of known and new variables that are of interest for further astrophysical investigations, in order to, e.g., search for additional bodies in eclipsing binary systems, or to test stellar interior models.

Altogether, 209,070 stars were monitored with BEST II during a total of 128 nights in 2009/2010. The overall variability fraction of 1.2–1.5% in these target fields is well comparable to similar ground-based photometric surveys. Within the main magnitude range of $R \in [11, 17]$, we identify 0.67(3)% of all stars to be eclipsing binaries, which indicates a completeness of about one third for this particular type in comparison to space surveys.

Subject headings: techniques: photometric — binaries: eclipsing — stars: variables

1. Introduction

The detailed study of variable stars is essential to astronomy, since it allows for the determination of stellar parameters such as mass, radius, luminosity, or temperature, as well as to study internal and external processes of stars, their compo-

sition, structure, and evolution. New detections not only broaden the statistical sample of variable stars, but are also important to gain further knowledge about the different processes that cause stellar variability.

The Berlin Exoplanet Search Telescopes, BEST (Rauer et al. 2004) and BEST II (Kabath et al. 2009a), are small-aperture, wide-field telescopes that are primarily used as a ground-based support for the CoRoT space mission (Baglin et al. 2006). Their observations help to exclude false positives from the list of transiting planetary candidates that are identified in time series from the satellite (Deeg et al. 2009; Rauer et al. 2010; Csizmadia et al. 2011). In addition, long-term photometric monitoring enables a precise characterization of stellar variability in CoRoT target fields (Karoff et al. 2007; Kabath et al. 2007, 2008, 2009a,b; Fruth et al. 2012; Klagyivik et al.

¹Institut für Planetenforschung, Deutsches Zentrum für Luft- und Raumfahrt, Rutherfordstr. 2, 12489 Berlin, Germany

²European Southern Observatory, Alonso de Córdova 3107, Vitacura, Casilla 19001, Santiago 19, Chile

³Astronomisches Institut, Ruhr-Universität Bochum, 44780 Bochum, Germany

⁴Instituto de Astronomía, Universidad Católica del Norte, Antofagasta, Chile

⁵Depto. Física, Universidad Católica del Norte, PO 1280, Antofagasta, Chile

⁶Zentrum für Astronomie und Astrophysik, Technische Universität Berlin, 10623 Berlin, Germany

2013) and beyond (Pasternacki et al. 2011).

During time periods not required for the regular CoRoT support, BEST II started an independent transit survey in 2009. Up to now, seven southern target fields have been monitored. While the analysis and follow-up of planetary candidates is ongoing, this paper presents a photometric analysis of stellar variability within the first three target fields of this survey.

The paper is organized as follows: Section 2 describes the telescope configuration and the observational data. Section 3 summarizes the data reduction and photometric analysis, while the search for stellar variability is outlined in Section 4. The results are presented in a large catalog of variable stars in Section 5, which includes a photometric classification of the variability type, ephemerides, a comparison with literature results for known cases, and a discussion on its limitations. Finally, Section 6 briefly summarizes the paper.

2. Telescope and Observations

BEST II is located at the Observatorio Cerro Armazones, Chile. Since 2007, it is operated continuously by the Institute of Planetary Research of the German Aerospace Center (DLR) in robotic mode from Berlin.

The system consists of a 25 cm Baker-Ritchey-Chrétien telescope with a focal ratio of $f/5.0$ and a $1^{\circ}7 \times 1^{\circ}7$ wide field of view (FOV). The photometric data presented here were obtained with a $4k \times 4k$ Finger Lakes Instrumentation CCD (IMG-16801E1) in white light, i.e., without any photometric filter. The CCD is most sensitive at $\lambda \approx 650$ nm, and the photometric system is roughly comparable to the Johnson R -band. The pixel size of $9 \mu\text{m}$ corresponds to an angular resolution of $1''.5 \text{ pixel}^{-1}$.

Three target fields, named F17, F18, and F19, have been monitored intensively with BEST II in 2009/2010. They have been selected by maximizing the total observing time weighted against the average airmass (Rauer et al. 2008, Equation 5) for each period of planned observations. For selecting F19, the simulation was complemented by additionally maximizing the number of target stars suitable for transit search (main sequence, less than 1% contamination). The stellar density of the fields differs significantly, since F17 and F19

are located close to the galactic plane ($|b| \approx 5^{\circ}$), while F18 is well outside ($b = -61^{\circ}$). The respective center coordinates of all three target fields are given in Table 1, which also lists the number of frames and light curves obtained in each pointing direction.

In total, BEST II collected 7,380 scientific frames and recorded light curves for 209,070 stars in these target fields. For the first field, F17, BEST II observations cover 39 photometric nights between 20/04/2009 and 22/07/2009. Field F18 was observed for 27 nights between 19/08/2009 and 27/10/2009, and field F19 for 62 nights between 24/03/2010 and 21/09/2010 (see Figure 1). When the observing coverage (colored areas in Figure 1) is related to the maximum available night time during these periods (gray areas), this corresponds to an average duty cycle of 35% for F17 and F19, and 38% for F18. Target fields F17 and F18 were observed with an exposure time of 120s, while 300s exposures were taken for F19; the typical cadence between two adjacent measurements is 2.5 minutes.

3. Data Reduction

The methods used here to obtain photometric time series from raw scientific images are part of a dedicated automated pipeline that has been applied before to various BEST/BEST II data sets (Karoff et al. 2007; Kabath et al. 2007, 2008, 2009a,b; Rauer et al. 2010; Pasternacki et al. 2011; Fruth et al. 2012; Klagyivik et al. 2013).

Calibration frames (bias, dark, flat) were recorded together with the observations and used in a standard reduction of instrumental effects. In order to increase the photometric precision in crowded fields, we apply the image subtraction algorithm (Alard & Lupton 1998; Alard 2000). For that, the calibrated scientific images are aligned to a common coordinate system, and the best ~ 20 – 40 scientific frames are stacked to a reference image. The latter is then fitted to individual frames and subtracted.

Simple unit-weight aperture photometry is used to extract both the flux from the reference frame and the relative flux in each subtracted frame. A standard radius of 5 pixels was chosen for target fields F17 and F19, while 7 pixels were used in the reduction of the less dense F18 field. An adjacent

Table 1: BEST II Target Field Information

| Field | Coordinates (J2000.0) | | Season | Nights | Frames | Stars | |
|-------|-----------------------|----------------------|-------------------|--------|--------|---------|----------------------|
| | α | δ | | | | Total | $\sigma \leq 0.01^m$ |
| F17 | $14^h 24^m 29^s$ | $-54^\circ 07' 20''$ | 20/04/09–22/07/09 | 39 | 2,259 | 68,317 | 3,170 |
| F18 | $22^h 52^m 00^s$ | $-44^\circ 12' 00''$ | 19/08/09–27/10/09 | 27 | 2,266 | 13,551 | 427 |
| F19 | $16^h 26^m 00^s$ | $-56^\circ 12' 00''$ | 24/03/10–21/09/10 | 62 | 2,855 | 127,202 | 10,120 |

NOTE.—Shown are the center coordinates, the time range between the first and last observing night, the number of good photometric nights with observations within this range, the number of acquired frames, and the number of total/low-noise light curves for each target field.

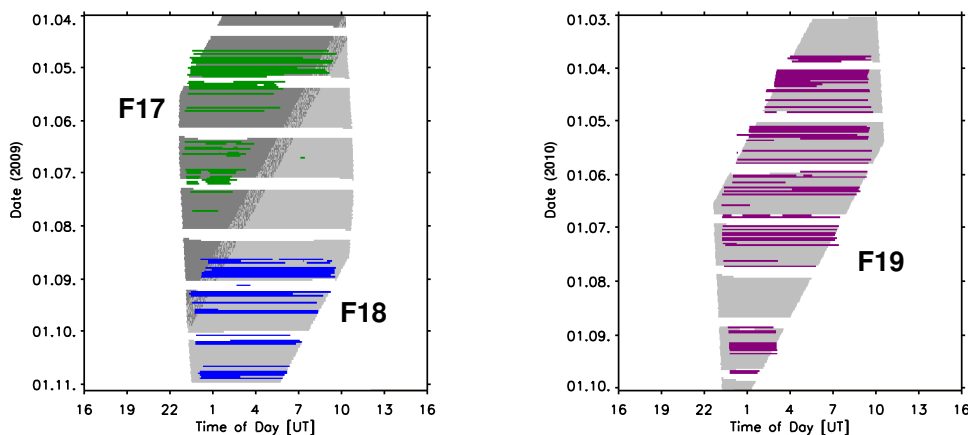


Fig. 1.— BEST II field observations during Chilean winters 2009 and 2010. Times of observations are shown for the fields F17 (green), F18 (blue), and F19 (violet). For comparison, gray areas indicate times with an *optimal* astronomical visibility, i.e., corresponding to each respective target field being observable at least 30° above the horizon, the Sun below -8° , and a Moon phase of less than 90% (cf. Rauer et al. 2008).

annulus up to an outer radius of 20 pixels is used for an estimation of the background flux. In order to remove global flux variations in the data, e.g., due to weather or nightly variations of the sky transparency, a comparison star is calculated out of some thousand light curves with the smallest photometric noise in each data set and then subtracted from each light curve.

Finally, all stars are matched with the UCAC3 catalog (Zacharias et al. 2010) in order to assign equatorial coordinates and to adjust instrumental magnitudes to a standard magnitude system. The astrometric calibration is obtained using the routines `grmatch` and `grtrans` by Pál & Bakos (2006); for the three data sets presented here, it achieves a match for $\sim 85\%$ of the stars with an average residual of $0''.2-0''.3$. The magnitude calibration is obtained by shifting each data set by the median difference between all instrumen-

tal magnitudes and their respective catalog value (R2MAG of UCAC3). Since the photometric systems are comparable but not identical, this calibration yields an accuracy of $\sim 0.3-0.5$ mag.

Brightness variation, however, can be measured to a much higher precision with BEST II. For the brightest stars in each data set, it obtains a noise level of ~ 3 mmag in unbinned data over the whole observing season. As an example, Figure 2 shows the standard deviation σ as a function of stellar magnitude for target field F17. Overall, BEST II obtained measurements with mmag-precision ($\sigma \leq 0.01$ mag) for 13,717 stars in the three target fields presented here (cf. Table 1).

4. Search for Variability

The three data sets were searched for stellar variability using a combination of the *J*-index

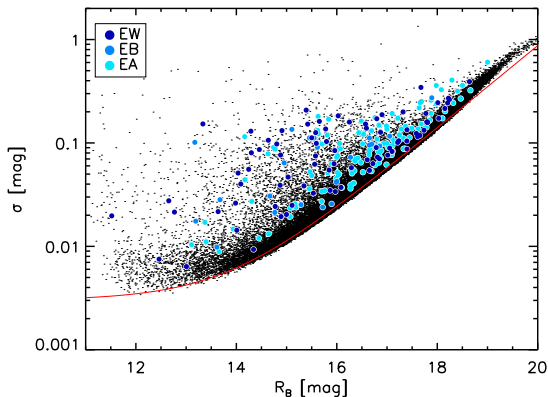


Fig. 2.— Photometric standard deviation σ in unbinned BEST II data as a function of the instrumental magnitude R_B (example for target field F17). Blue dots indicate binaries in the field (cf. Section 5), while the red line shows the minimum noise level $\sigma_{\min}(R_B)$ in this data set.

(Stetson 1996) and an analysis of variance period search (AoV; Schwarzenberg-Czerny 1996). The method and its parameters have been described in detail by Fruth et al. (2012).

First, the J -index is used to identify light curves that are clearly *not* variable. Using a limit $J < J_{\max}$, we excluded 93,583 non-variable stars; thereby, J_{\max} was set to 0.1 for the crowded target fields F17 and F19, while 0.05 was chosen for the less dense F18 field. Second, the remaining 115,487 light curves were each fitted with seven harmonics having fundamental periods within the range of 0.05–100 days (F17, F19) and 0.05–80 days (F18), respectively. Third, a modified ranking parameter q was calculated from the AoV statistic, whereby lower weights are given to periodic variability that is encountered in many light curves.

Finally, a total of 5,480 light curves with $q \geq 10$ were inspected visually for stellar variability (for the respective star count within each target field, see Table 2). This mainly included reviewing the overall signal-to-noise ratio (SNR), checking individual nights or events for systematic effects, inspecting the stellar neighborhood for possible sources of contamination, and analyzing alternative period solutions. The latter step lead us to adjust the initial ephemerides in several cases –

usually to multiples of the AoV period, e.g., due to primary and secondary eclipses of (slightly) different depths.

For some cases, the angular resolution of BEST II is not sufficient to fully separate the light of adjacent stars, and the photometric apertures overlap. Thus, variability of the same shape and period can be detected in multiple light curves. In order to constrain the source of variability, we carefully checked each of these *contaminated* objects using a smaller photometric aperture (3 Px radius).

Stellar crowding also leads to an overestimation of the instrumental magnitude and an underestimation of the amplitude of variability. In order to assess this effect quantitatively, we calculated the flux fraction within each photometric aperture i that does *not* originate from the respective target i as

$$\gamma_i = 1 - \frac{g_{ii}f_i}{\sum_j g_{ij}f_j} = 1 - \frac{g_{ii}}{\sum_j g_{ij}10^{0.4(m_i - m_j)}}, \quad (1)$$

whereby f_j denotes the flux of star j , m_j its magnitude, and g_{ij} describes the geometric integral of its PSF within the target aperture i (normalized, i.e., $g_{ij} \in [0, 1]$). The calculation of (g_{ij}) assumes Gaussian PSFs (3 Px FWHM) and circular apertures (radii as used for photometry), whereas R magnitudes from the NOMAD catalog (Zacharias et al. 2004) are used to estimate (m_j) . Due to missing catalog entries or magnitudes, the calculation of γ can be inaccurate or even fail in some cases. Also, its accuracy is affected by systematic effects such as the difference in the two photometric systems (BEST II and catalog), deviations of the PSF from a Gaussian shape, or long-term stellar variability. Thus, the automatically calculated γ value in Table 5 should only be taken as a first-order approximation.

5. Results

The visual inspection revealed 2,406 stars with clear and previously unknown variability. In addition to that, we confirm the known variability of 17 stars and suspect further 617 objects to be variable. For the latter group, the variability itself, its type, and/or period could not be determined without ambiguity. Predominantly, these are objects that show brightness variations close to the

noise level of their light curve. The numbers of detected, known, and suspected variables within each target field are summarized in Table 2.

5.1. Classification

Detected variable stars are assigned variability types following Sterken & Jaschek (1996) and the classification scheme of the General Catalog of Variable Stars (GCVS; Samus et al. 2009). The identification is solely based on photometry, i.e., it depends on the shape, amplitude, and period of the brightness variation.

The following classes could be identified:

- **Eclipsing binary systems.** Light curves with clear eclipses and almost no variation in between are classified as Algol-type binaries (EA; prototype β Per). For systems with ellipsoidal components, phase variations are significant and hinder an exact determination of the beginning/end of eclipses (EB type; β Lyr). At orbital periods below one day, both objects are in contact, eclipses are of equal depth and are fully blended with the phase variation (EW type; W UMa).
- **Pulsating variable stars.** From photometry, the following pulsating types could be identified: δ Scuti variables (DSCT; periods $p \leq 0.2$ days), RR Lyrae (RR; $p = 0.2$ –1 day, characteristic shape), Cepheids (CEP; $p > 1$ day, amplitudes 0.01–2 mag), Gamma Doradus stars (GDOR), and semi-regular variables (SR; $p \geq 20$ days with irregularities).
- **Rotating variable stars (ROT).** Stellar rotation can introduce flux variations, e.g., due to stellar spots, magnetic fields, or ellipsoidal components. Since BEST II photometry alone is usually not sufficient to distinguish these cases, they are grouped under a general "ROT" classification.
- **Long periodic variables (LP).** Non-periodic variables or stars variable on time scales comparable to/larger than the observational coverage are named LP.
- **Inconclusive Cases (VAR).** Stars showing clear variability that cannot be assigned

a type according to the classification scheme from photometry; further observations are needed to better constrain the physical origin of variability.

Details on how many stars have been found in each variability class and target field are given in Table 3. In total, 954 (plus 104 suspected) eclipsing binaries could be identified, 527 (139) pulsators, 200 (81) stars with rotational modulation, 344 (78) long periodic variables, and 398 (215) with other types of variability.

A figure set of all light curves is available in the online version of the journal. Figure 3 illustrates its form and content by highlighting examples that can be interesting for further astrophysical studies, such as, e.g., eclipsing binaries with a high SNR (F17_10421, F19_009645, F19_030794, F19_033571, F19_100160), eccentric eclipsing binaries (F19_055270, F19_100956), a cataclysmic binary (F19_022713), or RR Lyrae pulsators with amplitude modulation known as the Blazhko-effect (Blazhko 1907; F19_086712, F19_124221).

5.2. Known Variables

A total number of 17 variable stars contained in the BEST II data sets F17–F19 were previously known. Table 4 gives their identifiers and compares periods and classifications with the corresponding reference values. The light curves of UX Nor (F19_046530) and NSV 7658 (F19_098447) are shown as examples in Figure 3.

For *all* stars that were classified or have periods determined by previous studies, our results are in excellent agreement. For several known variables such as EM Nor (F19_104459), IX Nor (F19_107786), and PW Nor (F19_116322), we did not find a reference to a CCD light curve, so that this survey can be considered to provide the first high-accuracy photometric measurements of these objects. In the following text, we comment some new insights for individual cases.

BE Gru (F18_05548), AD Gru (F18_08895), and KK Nor (F19_088903). For the first time, the high precision of the new data allows to constrain the Blazhko-effect for these RR variables: Within our detection limit, we find no evidence for an amplitude modulation. This finding can be used, e.g., to study the frequency of the

Table 2: Number of Stars Identified as Variables in BEST II target fields F17–F19.

| FIELD | STARS | | | VARIABLE STARS | | |
|-------|---------|-------------------|--------------|----------------|---------------|-------------|
| | TOTAL | $J \geq J_{\max}$ | $q \geq 10$ | KNOWN | NEW | SUSPECTED |
| F17 | 68,317 | 20,965 (31%) | 1,126 (1.7%) | 2 | 639 (0.94%) | 179 (0.26%) |
| F18 | 13,551 | 5,399 (40%) | 176 (1.3%) | 4 | 13 (0.10%) | 7 (0.05%) |
| F19 | 127,202 | 89,123 (70%) | 4,178 (3.3%) | 11 | 1,754 (1.38%) | 431 (0.34%) |
| TOTAL | 209,070 | 115,487 (55%) | 5,480 (2.6%) | 17 | 2,406 (1.15%) | 617 (0.30%) |

NOTE.—For each field, the table gives the total number of light curves, the number of light curves selected for variable star search (with $J \geq J_{\max}$), the number of light curves that are finally analyzed visually (with variability parameter $q \geq 10$, cf. Fruth et al. 2012), and the number of known, new, and suspected variable stars. Numbers in brackets give the relative fraction compared to the total count.

Table 3: Star Counts per Variability Class.

| | EA | EB | EW | EW/DSCT | DSCT | RR | CEP | GDOR | ROT | SR | LP | VAR |
|-------|----------|----------|----------|----------|----------|---------|----------|-------|------------|----------|----------|-----------|
| F17 | 83 (9) | 24 (7) | 119 (6) | 41 (11) | 46 (23) | 40 (12) | 29 (9) | 1 (0) | 77 (38) | 14 (3) | 156 (56) | 11 (5) |
| F18 | 0 (1) | 0 (1) | 3 (0) | 0 (0) | 0 (0) | 6 (0) | 0 (0) | 0 (0) | 4 (4) | 0 (0) | 1 (0) | 3 (1) |
| F19 | 281 (30) | 127 (28) | 317 (22) | 97 (49) | 118 (31) | 53 (9) | 59* (6) | 0 (0) | 119** (39) | 161 (46) | 187 (22) | 246 (149) |
| Total | 364 (40) | 151 (36) | 439 (28) | 138 (60) | 164 (54) | 99 (21) | 87* (15) | 1 (0) | 200** (81) | 175 (49) | 344 (78) | 260 (155) |

*Including one CEP/EA

**Including one ROT/EA and one ROT/EB

NOTE.—Given are the numbers of known and newly detected variable stars for each field and variability class (suspected variables in brackets). Crowded cases are only counted once.

Table 4: Known variable stars in data sets F17–F19.

| IDENTIFIER | R_B | PERIOD P [d] | CLASSIFICATION | REFERENCE | | | |
|--------------|---------------------|----------------|----------------|-----------|-----|--------|-----------------------------|
| BEST II Ref. | [mag] | BEST II Ref. | BEST II Ref. | | | | |
| F17_03458 | ASAS J142013-5339.9 | 11.6 | 3.329(4) | 3.31 | ROT | ROT | Kiraga (2012) |
| F17_32682 | ASAS J142428-5416.0 | 12.5 | – | 323.7 | LP | MISC | Pojmanski (2002) |
| F18_02074 | ASAS J224935-4341.2 | 11.9 | – | 68.25 | LP | MISC | Pojmanski (2002) |
| F18_03793 | YZ Gru | 16.5 | 0.6976(7) | 0.6974 | RR | RRAB | Meinunger (1979) |
| F18_05548 | BE Gru | 14.1 | 0.6055(2) | 0.6054 | RR | RRAB | Meinunger (1979) |
| F18_08895 | AD Gru | 15.5 | 0.7592(5) | 0.7592 | RR | RRAB | Meinunger (1979) |
| F19_000499 | FV Nor | 12.6 | – | – | LP | LP? | Hoffleit (1931) |
| F19_045321 | NU Nor ^a | 11.7 | – | – | LP | L | Meinunger (1970) |
| F19_046530 | UX Nor | 12.1 | 2.386(2) | 2.38602 | CEP | CWB | Petersen & Andreasen (1987) |
| F19_088903 | KK Nor | 14.0 | 0.45493(6) | – | RR | RR | Meinunger (1970) |
| F19_089192 | EO Nor | 11.3 | 0.8523(3) | 0.8523(2) | EA | EA/SD: | Kruytbosch (1935) |
| F19_093711 | IZ Nor | 11.0 | – | – | LP | L | Meinunger (1970) |
| F19_098447 | NSV 7658 | 10.6 | – | – | LP | – | Luyten (1938) |
| F19_104459 | EM Nor | 11.2 | 0.7383(2) | 0.7384 | EW | EW | Malkov et al. (2006) |
| F19_107786 | IX Nor | 10.6 | – | – | LP | M | Meinunger (1970) |
| F19_111712 | UV Nor | 12.8 | 0.8742(2) | 0.8741 | EA | EA | Malkov et al. (2006) |
| F19_116322 | PW Nor | 12.1 | – | – | LP | M: | Luyten (1936) |

^aMeinunger (1970) assigns the variability of NU Nor to the star 2MASS 16274939-5533450 (BEST II F19_045485). However, in BEST II data, the variability can clearly be assigned to the object 2MASS 16275033-5533400 (BEST II F19_045321), which is located at an angular distance of $9''$ to the former.

NOTE.—Given are identifiers of this work and the GCVS and/or VSX, BEST II instrumental magnitudes R_B , and periods and classifications (if available) as obtained within this work and by previous surveys as referenced, respectively.

Blazhko-effect (e.g., Sódor et al. 2012) in order to gain a better understanding of this effect. For KKNor, the period was first determined within this work.

FV Nor (F19_000499). The long-periodic variability was first suspected by Hoffleit (1931) and is now clearly confirmed.

UX Nor (F19_046530). This object has one of the longest periods of RRab stars and thus is intensively studied (Walraven et al. 1958; Petit 1960; Diethelm 1983, 1986, 1990; Kwee & Diethelm 1984; Harris 1985; Petersen & Diethelm 1986; Petersen & Andreasen 1987; Moskalik & Buchler 1993; Sandage et al. 1994; Feuchtinger & Dorfi 1996). The high accuracy of the new data can help to better constrain theoretical models of these pulsations (see, e.g., Feuchtinger & Dorfi 1996).

NSV 7658 (F19_098447). This object was only suspected to be variable by Luyten (1938). Its long-term variability is now clearly confirmed.

IX Nor (F19_107786). The Mira nature of IX Nor is well compatible with our measurements. However, a period of its variability cannot be given since the observations do not cover a brightness maximum.

PW Nor (F19_116322). The Mira classification for PW Nor is only suspected by GCVS, but is also well supported by our measurements; they show a variation from ~ 12.3 to 9.8 mag during a half period lasting approx. 140 days.

5.3. Catalog of New Variables

Information on all known, newly detected, and suspected variable stars identified within the three BEST II data sets is provided in a star catalog. Table 5 shows a small extract for guidance regarding its form and content. The complete catalog in a machine-readable format as well as light curves for each star are available in the online journal. Photometric data and finding charts are available upon request.

Each star is identified by instrumental coordinates, as well as an internal BEST II and 2MASS

ID (if available); the latter refers to the closest 2MASS (Skrutskie et al. 2006) object within $2''$ distance from the respective BEST II coordinates. Instrumental magnitudes R_B are obtained without filter and should thus only be used for a broad approximation (cf. Section 3). Ephemerides and amplitudes of variability are given based on the results of the AoV algorithm (except for cases that were adjusted as a result of visual inspection, see Section 4). No ephemerides and amplitudes are given for long periodic (LP) classified variables.

Contaminated light curves are marked with a “c” flag in the catalog. If the origin of variation can clearly be assigned to one of the overlapping stars due to a sufficient angular separation and/or brightness difference, only one object is presented in the catalog. However, in 43 cases, two objects are too close to each other and are thus both presented as variables (marked with the corresponding ID under “other names” in Table 5, but not counted twice in Tables 2 and 3). Observations at higher angular resolution are needed to constrain the true origin of variability.

5.4. Catalog Characterization

The new variables of this study will increase the number of variables listed in the VSX catalog (246,007 as of 14/08/2013, including suspected) by 1.2%. For comparison, Table 6 shows the volume, yield, and magnitude range of this work, previous BEST/BEST II studies, and other large photometric surveys.

The detection yield of photometric surveys is subject to various systematic differences. Most importantly, these include the photometric precision, monitored magnitude range and FOV, the time span and duty cycle of observations, and the applied analysis techniques and selection criteria; for a discussion, see also Tonry et al. 2005. For ground-based projects, the detection yield typically ranges between 0.1% (OGLE-III) and 2.7% (ASAS-2), which compares well to the overall fraction of 1.2% variables (1.5% including suspected) identified in this study. However, the increased precision of space-based surveys indicates a much larger fraction of stars to be variable – McQuillan et al. (2012) detected clear periodic or quasi-periodic behaviour for 16% of stars in *Kepler* (Borucki et al. 2010) data, and Debosscher et al. (2009) estimated at least 40% of CoRoT light

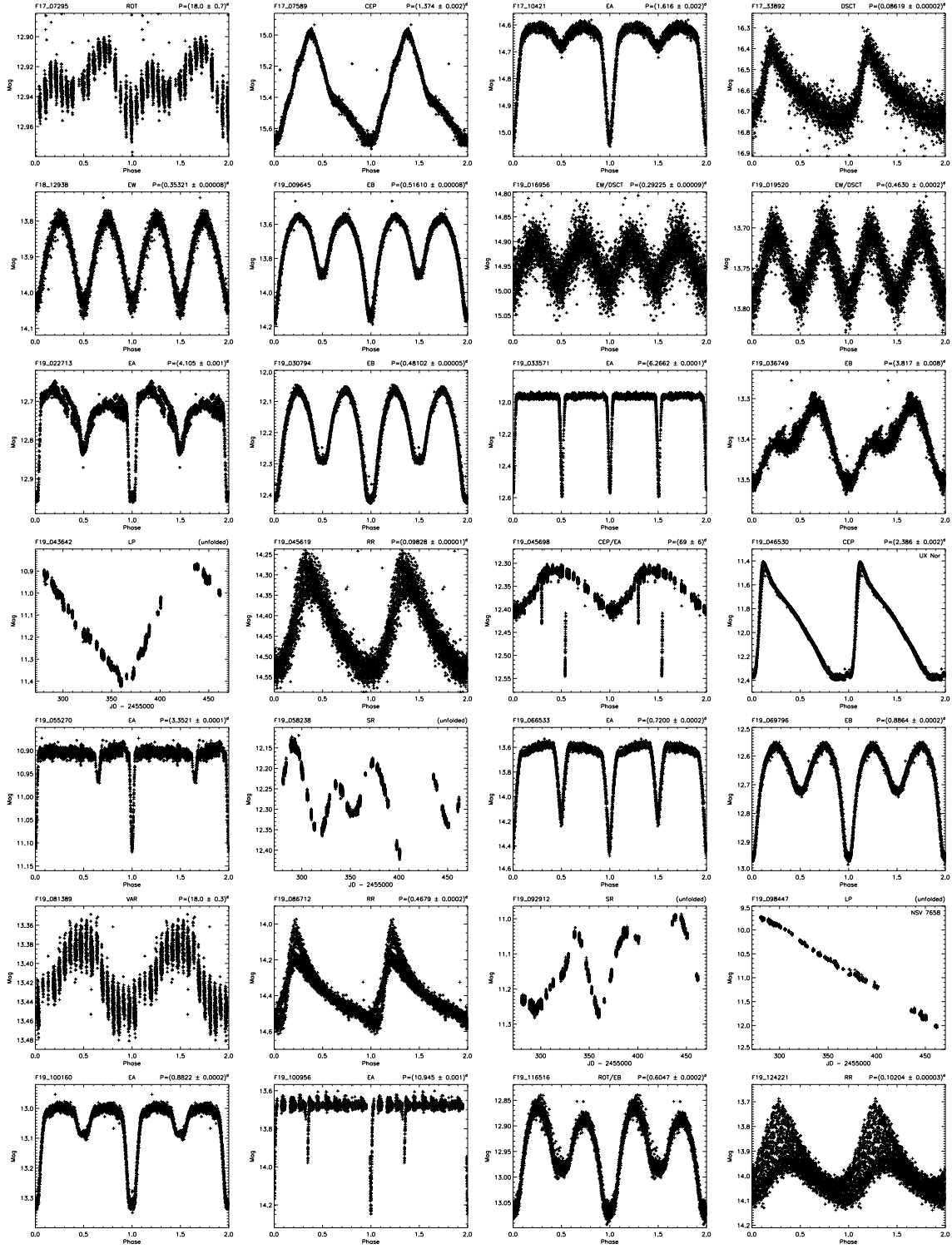


Fig. 3.— Light curves of variable stars in BEST II target fields F17–F19 (examples). (The complete figure set of 3,083 light curves is available in the online journal.)

TABLE 5
CATALOG OF VARIABLE STARS IN THREE SOUTHERN BEST II TARGET FIELDS (SELECTION)

| BEST II | flag | 2MASS | $\alpha(J2000.0)$ | $\delta(J2000.0)$ | R_B [mag] | T_0 [rHJD] | P [d] | A [mag] | γ [%] | Type | Other names |
|------------|-----------|------------------|---|-------------------|-------------|--------------|-------------------|---------------|--------------|---------|-------------|
| F17 | | | | | | | | | | | |
| F17_00273 | | 14190561-5357064 | 14 ^h 19 ^m 05.6 ^s | -53°57'06.4'' | 14.12 | -45.986 | 12.0 ± 0.3 | 0.024 ± 0.008 | 1 | ROT | |
| F17_00277 | | 14184206-5410596 | 14 ^h 18 ^m 42.1 ^s | -54°10'59.8'' | 14.40 | -52.708 | 19 ± 2 | 0.03 ± 0.02 | 0 | ROT | |
| F17_00346 | <i>s</i> | 14194815-5332206 | 14 ^h 19 ^m 48.1 ^s | -53°32'20.4'' | 14.59 | ... | ... | ... | 0 | LP | |
| F17_00411 | <i>s</i> | 14184782-5408336 | 14 ^h 18 ^m 47.8 ^s | -54°08'33.7'' | 12.77 | -35.920 | 13.5 ± 0.3 | 0.03 ± 0.02 | 0 | ROT | |
| F17_00448 | | 14195281-5330186 | 14 ^h 19 ^m 52.8 ^s | -53°30'18.6'' | 16.66 | -57.366 | 0.3055 ± 0.0002 | 0.21 ± 0.07 | 3 | EW | |
| F17_00521 | | 14194720-5334110 | 14 ^h 19 ^m 47.2 ^s | -53°34'10.9'' | 14.39 | ... | ... | ... | 14 | SR | |
| F18 | | | | | | | | | | | |
| F18_00214 | | 22471763-4420583 | 22 ^h 47 ^m 17.7 ^s | -44°20'58.6'' | 13.26 | 72.444 | 12.8 ± 0.4 | 0.032 ± 0.009 | 0 | VAR | |
| F18_10917 | | 22543478-4418014 | 22 ^h 54 ^m 34.8 ^s | -44°18'01.4'' | 14.02 | 63.543 | 0.642 ± 0.003 | 0.04 ± 0.03 | 0 | RR | |
| F19 | | | | | | | | | | | |
| F19_000002 | <i>c</i> | | 16 ^h 31 ^m 57.2 ^s | -56°46'40.0'' | 14.24 | 281.119 | 0.51944 ± 0.00009 | 0.59 ± 0.03 | ... | EB | |
| F19_000271 | | 16315167-5607312 | 16 ^h 31 ^m 51.7 ^s | -56°07'31.1'' | 14.35 | 299.145 | 64 ± 7 | 0.08 ± 0.02 | 9 | VAR | |
| F19_000396 | | 16315404-5636039 | 16 ^h 31 ^m 53.9 ^s | -56°36'04.7'' | 12.79 | 293.912 | 7.8905 ± 0.0001 | 0.16 ± 0.01 | 8 | EA | |
| F19_000433 | <i>c</i> | 16315321-5631219 | 16 ^h 31 ^m 53.2 ^s | -56°31'22.7'' | 12.31 | 475.611 | 69 ± 4 | 0.50 ± 0.05 | 5 | CEP | |
| F19_000441 | | 16315078-5608431 | 16 ^h 31 ^m 50.8 ^s | -56°08'42.8'' | 13.42 | 290.725 | 20.2 ± 0.8 | 0.03 ± 0.02 | 12 | ROT | |
| F19_000499 | <i>ck</i> | 16315094-5614576 | 16 ^h 31 ^m 51.0 ^s | -56°14'57.9'' | 12.60 | ... | ... | ... | 0 | LP | FV Nor |
| F19_000546 | | 16314493-5527070 | 16 ^h 31 ^m 44.9 ^s | -55°27'07.0'' | 15.52 | 280.778 | 0.24814 ± 0.00007 | 0.3 ± 0.2 | 59 | EW/DSCT | |
| F19_000944 | | | 16 ^h 31 ^m 44.9 ^s | -55°44'46.8'' | 15.47 | 280.712 | 0.5124 ± 0.0004 | 0.07 ± 0.05 | 78 | EA | |
| F19_041783 | <i>c</i> | 16280785-5524442 | 16 ^h 28 ^m 07.8 ^s | -55°24'44.3'' | 15.07 | 281.033 | 0.3947 ± 0.0002 | 0.08 ± 0.05 | 46 | EW | F19_041855 |
| F19_041855 | <i>c</i> | 16280761-5524508 | 16 ^h 28 ^m 07.6 ^s | -55°24'50.9'' | 15.12 | 281.029 | 0.3947 ± 0.0003 | 0.07 ± 0.04 | 72 | EW | F19_041783 |

NOTE.—Table 5 is published in its entirety in the electronic edition of the *Astronomical Journal*. A portion is shown here for guidance regarding its form and content.

Stars have been matched with the closest 2MASS object within a radius of 2 arcseconds. Coordinates are given for epoch J2000.0 and were derived by an astrometric match of CCD to UCAC3 coordinates. Given magnitudes are instrumental and reflect the CCD sensitivity, as observations have been obtained without filter. Overlapping apertures of neighboring stars can lead to contaminated light curves – such cases are marked with a 'c' flag. Suspected variables are marked by 's', whereas previously known variables are marked by 'k' (see also Section 5.2 and Table 4). Amplitudes A and ephemerides (variability period P and times of minimum brightness T_0 , given in rHJD=HJD-2455000) are the results of the AoV algorithm. The contamination parameter γ approximates the fraction of light in the target's aperture coming from other objects than the target itself (see text).

TABLE 6
VARIABLE STAR DETECTION YIELD IN COMPARISON TO OTHER SURVEYS.

| Project | N_{\star} | N_{var} | N_{var}/N_{\star} | Mag | References |
|----------------------------|-------------------|------------------|----------------------------|-----------|---|
| BEST/BEST II | | | | | |
| BEST | 121,811 | 335 | 0.28% | 11–15 | Karoff et al. (2007); Kabath et al. (2007, 2008); Pasternacki et al. (2011) |
| BEST II (CoRoT) | 218,809 | 1,107 | 0.51% | 11–17 | Kabath et al. (2009a,b); Fruth et al. (2012) |
| BEST II (F17–F19) | 209,070 | 3,040 | 1.45% | 11–17 | This work |
| OTHER GROUND-BASED SURVEYS | | | | | |
| UNSW | 87,000 | 850 | 0.98% | 8–14 | Christiansen et al. (2008) |
| HAT 199 | 98,000 | 1,617 | 1.65% | 8–14 | Hartman et al. (2004) |
| EROS II | 1,913,576 | 1,362 | 0.07% | 11–17 | Derue et al. (2002) |
| ASAS-2 | 140,000 | 3,800 | 2.71% | 8–13 | Pojmanski (2000) |
| ASAS-3 | $1.7 \cdot 10^7$ | 50,099 | 0.29% | 8–14 | Paczyński et al. (2006) |
| OGLE-II | $1.65 \cdot 10^7$ | 68,194 | 0.41% | ≤ 20 | Zebrun et al. (2001) |
| OGLE-III | $2 \cdot 10^8$ | 193,000 | 0.10% | 12–20 | Soszyński et al. (2008, 2011) |
| SPACE-BASED SURVEYS | | | | | |
| CoRoT (first 4 fields) | 39,659 | | $\sim 40\%$ | 12–16 | Debosscher et al. (2009) |
| Kepler | 156,000 | | | 9–16 | Borucki et al. (2011) |
| (quasi-)periodic | | | 16% | | McQuillan et al. (2012) |
| eclipsing binaries | 1,879 | | 1.2% | | Slawson et al. (2011) |

NOTE.—The table gives the number of surveyed stars N_{\star} , the number of found variables N_{var} , and the corresponding ratio N_{var}/N_{\star} for BEST/BEST II publications, this work, and selected references of important variable star surveys. If noted in the publication, N_{var} here includes known and new detections, i.e., the whole detection yield of a given survey. The column "Mag" gives each survey's approximate magnitude range.

curves to be variable.

In the following text, the sensitivity of this study is investigated as a function of its three most important limitations, namely, the magnitude range, the SNR, and the period range.

5.4.1. Magnitude Range and Variable Fraction

In order to evaluate the completeness of our study as a function of apparent brightness, we compared the number of observed stars against the GSC2.2 catalog (Lasker et al. 2008), which resembles our results the best within the given magnitude range among several catalogs tested. Differences between the instrumental photometric system R_B and the R band of GSC2.2 were corrected for by subtracting the average difference $\langle \Delta m \rangle$ to obtain

$$R'_B = R_B - \langle \Delta m \rangle, \quad (2)$$

whereby $\Delta m = R_B - R$.

Figure 4 compares the number of catalog stars (within bins of 0.2 mag) with the respective numbers for each target field of this work. The latter is shown both for all stars and a reduced sample having $|\Delta m| < 0.5$ mag, since large deviations may in-

dicate a systematic disagreement, e.g., due to different angular resolutions. The comparison shows a very good agreement between catalog and survey stars ($\gtrsim 80\%$ completeness) within the magnitude range of $11 \lesssim R \lesssim 17$ for the two data sets F17 and F18. For target field F19, a similarly good agreement is confined to the range of $13 \lesssim R \lesssim 16$, since most stars with $R \lesssim 13$ are saturated (due to the longer exposure time compared to F17 and F18), and stars with $R \gtrsim 16$ are more strongly affected by crowding in this dense target field.

Figure 5 shows the number of variables and suspected variables N_{var} identified within this work as a fractional ratio of all stars N_{\star} per magnitude bin separated into binaries and other types. Naturally, the detection yield strongly decreases towards fainter magnitudes as the light curve precision decreases (cf. Figure 2). It peaks at 0.836(4)% for the binaries ($R_B \in [13, 14]$) and at 5.47(8)% for other types of variability ($R_B \in [11, 12]$). These values can be considered an overall lower limit of the real fraction of variable stars in our target fields, assuming that the physical dependency on the apparent brightness is small. Within the most sensitive magnitude range of this survey at

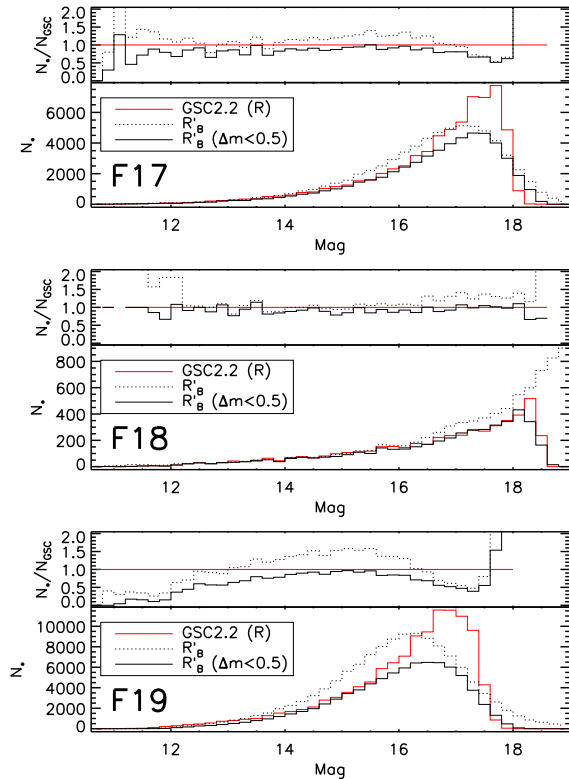


Fig. 4.— Magnitude histogram for each BEST II target field (in bins of 0.2 mag). The lower panel shows the number of stars N_* as a function of the GSC2.2 catalog R magnitude ($N_* \equiv N_{\text{GSC}}$; red), BEST II instrumental magnitude R'_B (Eq. 2; black dotted), and of BEST II stars with $|\Delta m| < 0.5$ mag (black). The upper panel shows the corresponding ratio N_*/N_{GSC} .

$11 \leq R_B \leq 17$, we identified an average fraction of 0.67(3)% eclipsing binaries. This compares well to the results of other photometric surveys such as OGLE, which identified an eclipsing binary fraction of ~ 0.5 – 0.6% ($I \in [14, 17]$; Graczyk et al. 2011, cf. their Figure 2). However, the fraction is significantly smaller compared to space surveys: Slawson et al. (2011) reported $\sim 2.0\%$ eclipsing binaries at comparable galactic latitudes in the *Kepler* field. If the latter approximately resembled the physical content in our target fields, the fraction of eclipsing binaries identified in this survey would correspond to a completeness of about one third for $R_B \in [11, 17]$.

5.4.2. SNR Limit

In order to evaluate our detection threshold, the amplitude A of each variable star is compared with the minimum noise level $\sigma_{\text{min}}(R_B)$, which is determined for each field from a fit to the lower noise limit in the (R_B, σ) -diagram (cf. Figure 2; after an analytical expression by Newberry 1991, Eq. 12).

Figure 6 shows a histogram of the SNR A/σ_{min} for eclipsing binaries and other types of variables. For the eclipsing binaries, the detection yield strongly increases for $A/\sigma_{\text{min}} \gtrsim 2$, while some types with a more sinusoidal variation such as DSCT can already be detected at $A/\sigma_{\text{min}} \gtrsim 1$. Note that σ_{min} here refers to *unbinned* data, although a large number of single measurements effectively contribute to each detection, thus increasing the SNR significantly.

5.4.3. Period Range

The duty cycle of any photometric survey significantly constrains its detection efficiency, in particular for variability at large time scales. Figure 7 shows the number of variables detected in this work as a function of their period. For comparison, the observational phase coverage $\phi_1(P)$ is shown for each target field. Since the detection of detached eclipsing binaries (EA) usually requires an observation of three or more of the relatively short eclipses, the right panel of Figure 7 shows the phase coverage $\phi_3(P)$ of at least three (infinitesimally short) events.

Figure 7 shows that our detection efficiency is largely confined to periods of $P \lesssim 10$ days in the case of eclipsing binaries, while the more regular periodic variability of other types can be detected up to $P \lesssim 100$ days. Qualitatively, the decrease in efficiency well follows the single and triple observational phase coverage, respectively. Furthermore, the period ranges of several distributions reflect their class definition (e.g., DSCT variables with $P \leq 0.2$ – 0.3 days). The observed peak of contact binaries (EW) at $P \approx 0.3$ – 0.4 days agrees well with recent findings of other surveys (e.g., ASAS, Paczyński et al. 2006; *Kepler*, Slawson et al. 2011; OGLE, Pietrukowicz et al. 2013).

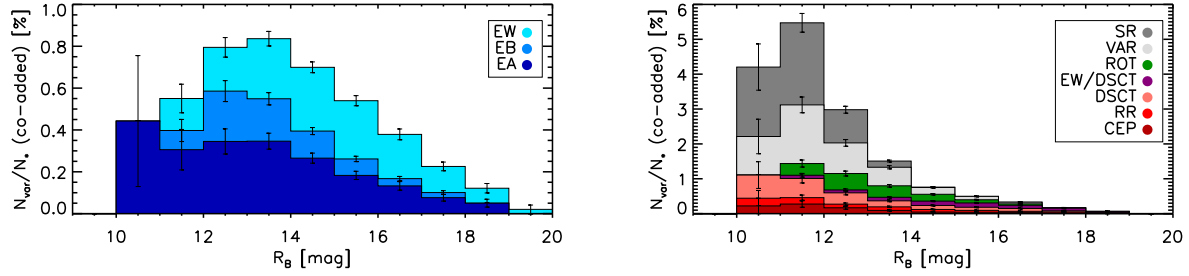


Fig. 5.— Ratio of the variable star count N_{var} (including suspected variables) and the total number N_{\star} of field stars as a function of R_B within bins of 1 mag. The left panel shows eclipsing binaries, while the right panel shows all remaining major classes. Bins are co-added, i.e., one complete bar refers to the total fraction of *all* classes. Vertical bars indicate the uncertainties of N_{var}/N_{\star} (assuming a Poisson distribution for both N_{var} and N_{\star}).

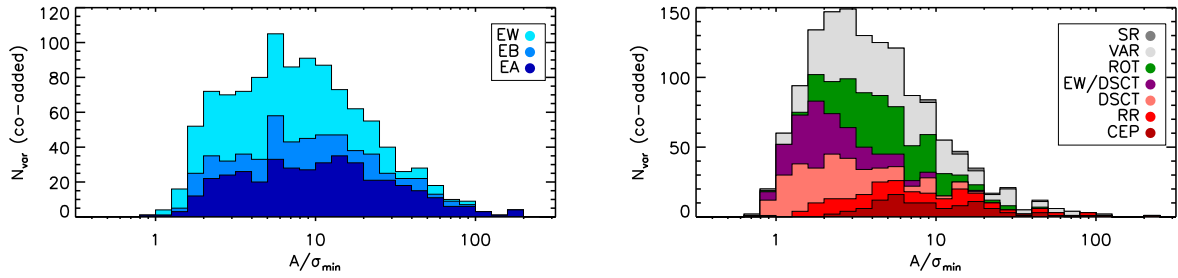


Fig. 6.— Variable star count N_{var} (including suspected) as a function of $\text{SNR} = A/\sigma_{\text{min}}$ in unbinned data (bin size $0.1 \log_{10}(A/\sigma_{\text{min}})$). The amplitudes A are taken from Table 5, while σ_{min} refers to the minimum noise level encountered at each respective magnitude (red line in Figure 2). Types, colors and co-adding as in Figure 5.

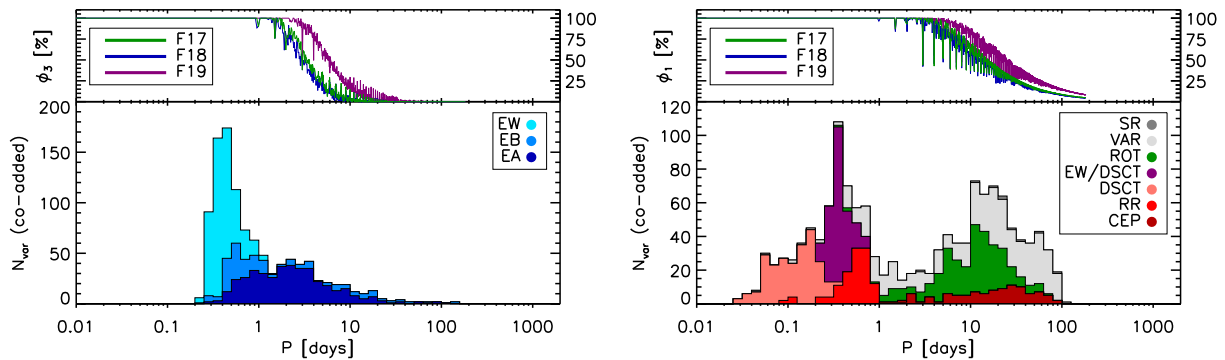


Fig. 7.— Variable star count N_{var} (including suspected) as a function of the period of variability P (see Table 5; bin size $0.1 \log_{10}(P/\text{days})$). The upper section of both panels shows the single and triple phase coverage, ϕ_1 and ϕ_3 , respectively, calculated from observing times of each field (cf. Figure 1). Colors and co-adding as in Figure 5.

6. Summary

A BEST II photometric survey of 209,070 stars within three Southern target fields revealed 2,423 variable objects (from which 17 were previously known) and an additional 617 stars which are suspected to be variable. The underlying stellar sample is most complete ($\gtrsim 80\%$) within the magnitude range of $R \in [13, 16]$ and the survey is most sensitive to detect eclipsing binaries up to periods of ~ 10 days and other types up to ~ 100 days. The average fraction of 0.67(3)% eclipsing binaries at magnitudes $R \in [11, 17]$ agrees well with other ground-based surveys and indicates a detection completeness of about one third in comparison to the more sensitive space surveys.

All information that is available from our photometric measurements of variable stars is presented in a large catalog, including the type and/or periodicity of the variability (if determinable). The catalog encompasses a number of objects that are very interesting for further astrophysical studies beyond the scope of this paper.

Acknowledgments. This work was funded by Deutsches Zentrum für Luft- und Raumfahrt and partly by the Nordrhein-Westfälische Akademie der Wissenschaften. Our research made use of the 2MASS, USNO-A2, NOMAD, GSC2.2, and GCVS catalog, the AAVSO variable star search index and the SIMBAD database, operated at CDS, Strasbourg, France.

REFERENCES

- Alard, C. 2000, *A&AS*, 144, 363
- Alard, C., & Lupton, R. H. 1998, *ApJ*, 503, 325
- Baglin, A., Auvergne, M., Barge, P., et al. 2006, in *The COROT Mission Pre-Launch Status*, ed. M. Fridlund, A. Baglin, J. Lochard, & L. Conroy, ESA SP-1306, 33–37
- Blažko, S. 1907, *Astronomische Nachrichten*, 175, 325
- Borucki, W. J., Koch, D., Basri, G., et al. 2010, *Science*, 327, 977
- Borucki, W. J., Koch, D. G., Basri, G., et al. 2011, *ApJ*, 736, 19
- Christiansen, J. L., Derekas, A., Kiss, L. L., et al. 2008, *MNRAS*, 385, 1749
- Csizmadia, Sz., Moutou, C., Deleuil, M., et al. 2011, *A&A*, 531, A41
- Debusscher, J., Sarro, L. M., López, M., et al. 2009, *A&A*, 506, 519
- Deeg, H. J., Gillon, M., Shporer, A., et al. 2009, *A&A*, 506, 343
- Derue, F., Marquette, J.-B., Lupone, S., et al. 2002, *A&A*, 389, 149
- Diethelm, R. 1983, *A&A*, 124, 108
- . 1986, *A&AS*, 64, 261
- . 1990, *A&A*, 239, 186
- Feuchtinger, M. U., & Dorfi, E. A. 1996, *A&A*, 306, 837
- Fruth, T., Kabath, P., Cabrera, J., et al. 2012, *AJ*, 143, 140
- Graczyk, D., Soszyński, I., Poleski, R., et al. 2011, *Acta Astron.*, 61, 103
- Harris, H. C. 1985, *AJ*, 90, 756
- Hartman, J. D., Bakos, G., Stanek, K. Z., & Noyes, R. W. 2004, *AJ*, 128, 1761
- Hoffleit, D. 1931, *Harvard College Observatory Bulletin*, 884, 10
- Kabath, P., Eigmüller, P., Erikson, A., et al. 2007, *AJ*, 134, 1560
- . 2008, *AJ*, 136, 654
- Kabath, P., Fruth, T., Rauer, H., et al. 2009a, *AJ*, 137, 3911
- Kabath, P., Erikson, A., Rauer, H., et al. 2009b, *A&A*, 506, 569
- Karoff, C., Rauer, H., Erikson, A., et al. 2007, *AJ*, 134, 766
- Kiraga, M. 2012, *Acta Astron.*, 62, 67
- Klagyivik, P., Csizmadia, Sz., Pasternacki, T., et al. 2013, *ApJ*, 773, 54

- Kruytbosch, W. E. 1935, *Bull. Astron. Inst. Netherlands*, 7, 253
- Kwee, K. K., & Diethelm, R. 1984, *A&AS*, 55, 77
- Lasker, B. M., Lattanzi, M. G., McLean, B. J., et al. 2008, *AJ*, 136, 735
- Luyten, W. J. 1936, *Astronomische Nachrichten*, 258, 121
- . 1938, *Publications of the Astronomical Observatory University of Minnesota*, vol. 2, no. 6
- Malkov, O. Y., Oblak, E., Snegireva, E. A., & Torra, J. 2006, *A&A*, 446, 785
- McQuillan, A., Aigrain, S., & Roberts, S. 2012, *A&A*, 539, A137
- Meinunger, I. 1970, *Zentralinstitut für Astrophysik Sternwarte Sonneberg, Mitteilungen über Veränderliche Sterne*, 5, 156
- . 1979, *Veröffentlichungen der Sternwarte Sonneberg*, 9, 107
- Moskalik, P., & Buchler, J. R. 1993, *ApJ*, 406, 190
- Newberry, M. V. 1991, *PASP*, 103, 122
- Paczynski, B., Szczygieł, D. M., Pilecki, B., & Pojmański, G. 2006, *MNRAS*, 368, 1311
- Pál, A., & Bakos, G. Á. 2006, *PASP*, 118, 1474
- Pasternacki, T., Csizmadia, Sz., Cabrera, J., et al. 2011, *AJ*, 142, 114
- Petersen, J. O., & Andreasen, G. K. 1987, *A&A*, 176, 183
- Petersen, J. O., & Diethelm, R. 1986, *A&A*, 156, 337
- Petit, M. 1960, *Annales d’Astrophysique*, 23, 681
- Pietrukowicz, P., Mróz, P., Soszyński, I., et al. 2013, *Acta Astron.*, 63, 115
- Pojmanski, G. 2000, *Acta Astron.*, 50, 177
- . 2002, *Acta Astron.*, 52, 397
- Rauer, H., Eislöffel, J., Erikson, A., et al. 2004, *PASP*, 116, 38
- Rauer, H., Fruth, T., & Erikson, A. 2008, *PASP*, 120, 852
- Rauer, H., Erikson, A., Kabath, P., et al. 2010, *AJ*, 139, 53
- Samus, N. N., Durlevich, O. V., Kazarovets, E. V., et al. 2009, *VizieR Online Data Catalog*, B/GCVS
- Sandage, A., Diethelm, R., & Tammann, G. A. 1994, *A&A*, 283, 111
- Schwarzenberg-Czerny, A. 1996, *ApJ*, 460, L107
- Skrutskie, M. F., Cutri, R. M., Stiening, R., et al. 2006, *AJ*, 131, 1163
- Slawson, R. W., Prša, A., Welsh, W. F., et al. 2011, *AJ*, 142, 160
- Sódor, Á., Jurcsik, J., Molnár, L., et al. 2012, in *Astronomical Society of the Pacific Conference Series*, Vol. 462, *Progress in Solar/Stellar Physics with Helio- and Asteroseismology*, ed. H. Shibahashi, M. Takata, & A. E. Lynas-Gray, 228
- Soszyński, I., Poleski, R., Udalski, A., et al. 2008, *Acta Astron.*, 58, 163
- Soszyński, I., Udalski, A., Pietrukowicz, P., et al. 2011, *Acta Astron.*, 61, 285
- Sterken, C., & Jaschek, C. 1996, *Light Curves of Variable Stars, A Pictorial Atlas*, ed. Sterken, C. & Jaschek, C. (Cambridge University Press)
- Stetson, P. B. 1996, *PASP*, 108, 851
- Tonry, J. L., Howell, S. B., Everett, M. E., et al. 2005, *PASP*, 117, 281
- Walraven, T., Muller, A. B., & Oosterhoff, P. T. 1958, *Bull. Astron. Inst. Netherlands*, 14, 81
- Zacharias, N., Monet, D. G., Levine, S. E., et al. 2004, in *Bulletin of the American Astronomical Society*, Vol. 36, *AAS 205th Meeting: Visible-Light Telescopes, Instruments, and Technology (Session 48)*, 1418
- Zacharias, N., Finch, C., Girard, T., et al. 2010, *AJ*, 139, 2184
- Zebrun, K., Soszynski, I., Wozniak, P. R., et al. 2001, *Acta Astron.*, 51, 317

